Atomic two-level states and relaxations observed in a computer model of amorphous $Ni_{81}B_{19}$

Leon D. van Ee, Barend J. Thijsse, and Jilt Sietsma

Laboratory of Materials Science, Delft University of Technology, Rotterdamseweg 137, 2628 AL Delft, The Netherlands

(Received 16 June 1997)

We study the atomic motion associated with low-frequency localized vibrational modes in a computer model of amorphous $Ni_{81}B_{19}$. We observe that the excitation of such a mode can lead to a transition of the system into a nearby potential-energy minimum. Such a ''jump'' has a cooperative character involving some tens of atoms. During the jump the potential-energy changes for atoms located at the jump site can be considerably larger than the total introduced excitation energy. The jumps are shown to take place at sites where so-called two-level states are located, whose existence in noncrystalline matter has been experimentally verified. The jumps can be of a reversible or of an irreversible nature, and a distinction can be made between two-level states that allow reversible atomic motion to take place and two-level states that disappear after the jump. The jumps can be identified with the local relaxations that have been predicted to occur in amorphous materials between 2 and 10 K and are correlated to low-frequency localized modes. The existence of double-well locations is argued to play an important role in diffusion at elevated temperatures, because they are sites that have a potentially high atomic mobility. [S0163-1829(98)04601-3]

I. INTRODUCTION

It is well known that at low temperatures ($T < 1$ K) glasses have a higher heat capacity and a lower thermal conductivity than crystals of the same composition.[1,2] This anomalous behavior can be explained by assuming that the dominant low-frequency contribution to the vibrational density of states is due to two-level states (TLS's).[3] According to this theory an atom or a group of atoms can occupy either of two (or more) potential-energy minima, which are separated by a low-energy barrier and are situated at a small distance from one another. The atoms can tunnel (or jump) between the two adjacent minima. The theory has been experimentally verified,[3] and TLS's appear to have a universal nature which is seen in many different amorphous materials. However, the theory does not give an indication of the type of local geometry that gives rise to the presence of TLS's, and what kind of atomic motion can take place at these sites.

Above 2 K the TLS's contribution to the heat capacity vanishes, but one does find an increase in the heat capacity between 2 to 10 K. Neutron measurements on vitreous silica[4] and metallic glasses[5] have shown these excitations to be harmonic vibrations which become increasingly anharmonic towards lower frequencies. Using the soft potential model as an extension of the TLS theory, Buchenau *et al.* show that these vibrations are localized on 10 to 100 atoms.[6] They explain the excitations at the low-frequency end, where the vibrations become anharmonic, by assuming additional thermally activated relaxations to take place, but their work gives no further insight in the nature of these processes.

In recent years low-frequency localized modes (also called resonant or quasilocalized modes) have also been observed in simulated glasses.[7–9] They are shown to be located at sites that differ significantly from the average glass structure. In search for the existence of multiple potential-energy minima, Guttman and Rahman[10] studied a low-frequency vibrational mode in a molecular-dynamics model of amorphous SiO_2. They moved the 11 oxygen atoms that had the largest amplitude eigenvectors in this mode in equal steps in the directions of these vectors. All other atoms were allowed to relax, reacting to the forced movement of the 11 atoms. A small secondary minimum in the potential energy was observed, indicating the presence of a TLS. Recently, using a computational model of amorphous Se, Oligschleger and Schober[11] showed that thermally activated local relaxations are strongly correlated to sites where localized low-frequency vibrational modes appear. To summarize, one finds clear indications that low-frequency localized modes play an important role in the low-temperature physics of amorphous materials. However, there is no direct insight in the nature of these modes.

This paper addresses two questions concerning low-frequency localized modes. First, are multiple potential-energy minima present at sites where low-frequency localized modes are located? Secondly, what kind of atomic motion can take place at these sites? Using molecular dynamics, we set low-frequency localized vibrational modes into motion in a physically consistent way. It will be shown that there is a relation between double potential-energy minima and atoms that can be identified, in the harmonic approximation, as principal participants in low-frequency localized vibrational modes. Putting such a mode into motion can lead to a cooperative atomic jump over an energy barrier rather than to vibrational motion around the original equilibrium locations. Although it is tempting to assume that a double well is a location where one or more atoms can jump from one minimum to the other without significant interference from the surrounding atoms and without affecting the possibility to reach the initial minimum by a similar reverse jump, we will show that in a glass this is an oversimplification. The surrounding atoms play a very important role in the process, allowing the potential-energy exchange among the atoms involved to be much larger than the barrier energy. Furthermore, most of the jumps have an irreversible nature, making it impossible for the system to jump back to the minimum from which it started.

II. SIMULATION PROCEDURES

The amorphous $Ni_{81}B_{19}$ system consists of $N = 2500$ atoms in a cubic box with periodic boundaries. Molecular-

dynamics (MD) runs were carried out at atmospheric pressure and at several constant temperatures. The equations of motion are solved using the velocity-Verlet algorithm with a time step of $\Delta t = 1.77$ fs. The total potential energy of the system V is expressed as

$$V = U + V_c(\rho) = \sum_{i=1}^{N} u^i + V_c(\rho)$$

$$= \frac{1}{2} \sum_{i=1}^{N} \sum_{i'=1}^{N} \Phi^{n,n'}(r^{i,i'}) + V_c(\rho), \quad (1)$$

where $V_c(\rho)$ is the cohesive contribution, which only depends on the density ρ, U is the pair potential energy, given by the sum of the pair potential energies u^i over all atoms i resulting from the effective pair potential interaction $\Phi^{n,n'}$, n is the type of atom i, and $r^{i,i'}$ is the distance between the atoms i and i'. For the effective pair potential we use the form

$$\Phi^{n,n'}(r)$$

$$= \begin{cases} A[(ar)^{-p} - (br)^{-q}]\exp[(ar-c)^{-1}] & (0 < r < c/a), \\ 0 & (r \geq c/a), \end{cases}$$

(2)

in which the parameters A, a, b, c, p, and q are positive and depend on the types n and n' of the atoms being considered (Weber and Stillinger[12]). These potentials have the advantages that no spherical cutoff is needed (this is important when performing low-temperature simulations) and that the potentials and their derivatives have no discontinuities in r. Starting from the potentials presented by Hausleitner and Hafner,[13] modified with data from Li *et al.*[14] (see Ref. 15), the parameters were empirically modified in order to obtain a system that (i) has partial reduced radial distribution functions that show a very good agreement with the experimental data of Lamparter *et al.*[16] for the same glass, (ii) has a density close to the experimentally measured number density ($\rho = 103$ nm^{-3}) at room temperature, and (iii) shows no segregation of B atoms.[13,15] The resulting parameters are given in Table I and the number density is 97.8 nm^{-3} at 304 K. Note the strongly nonadditive character of these potentials.

The usual method of obtaining an amorphous configuration as a starting point for a MD simulation is by quenching the liquid to a low temperature. Due to the maximum available time span in a simulation, this quench must be executed with a quenching rate that is too high to be experimentally achievable. In an alternative approach we obtain the starting configuration by applying the reverse Monte Carlo (RMC) method.[17,18] This method is shown to yield a more realistic starting structure than quenching a liquid.[15] Using the experi-
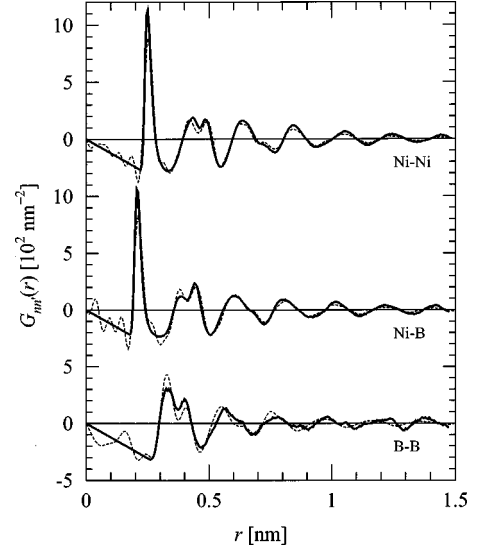

FIG. 1. Partial reduced radial distribution functions $G_{nn'}(r)$ of the MD system at 304 K averaged over 201 configurations covering a period of $t = 1.4$ ns (solid curve), compared with the experimental data of Lamparter (dashed curves) (Ref. 16) corrected for normalization errors. This correction consists of a multiplication of $G_{NiNi}(r)$, $G_{NiB}(r)$, and $G_{BB}(r)$ by 0.9699, 0.7544, and 0.8246, respectively (Ref. 18).

mental reduced partial radial distribution functions of Lamparter *et al.*,[16] the RMC method is applied to an initial equilibrium liquid configuration (1213 K) at high pressure in order to reach a number density $\rho = 97.8$ nm^{-3}. The RMC method does not use potential energies and in order to fine-tune the starting structure for the used pair potentials, the application of the RMC method was interrupted two times for a short (70 ps) MD simulation at 304 K.

III. SYSTEM CHARACTERISTICS

The partial reduced radial distribution functions $G_{NiNi}(r)$, $G_{NiB}(r)$, and $G_{BB}(r)$ of the model system at $T = 304$ K are shown in Fig. 1 together with the experimental data from Lamparter *et al.*[16] Only slight differences occur, mainly in the height of the first peaks and in the splitting of the second peaks. The distribution function $G_{BB}(r)$ for the MD system does not show enough structure, especially in the long range order. This is probably caused by the small well depth of the B-B potential (Table I), which was necessary to avoid the segregation of the B atoms. Despite these small differences, the overall agreement is very good and provides strong support for the chosen pair potentials and the use of the RMC method to obtain the initial configuration.

The partial vibrational densities of states $J_n(\omega)$ for atoms

TABLE I. Parameters of the pair potentials used for amorphous Ni$_{81}$B$_{19}$ [Eq. (2)]. The quantities r_{min} and Φ_{min} refer to the bottom of the pair potential-energy well.

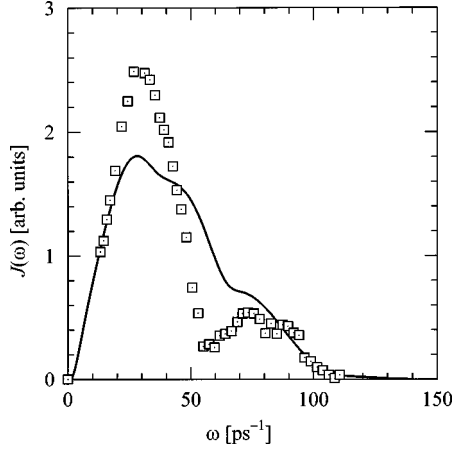| n-n'	A [eV]	a [nm^{-1}]	b [nm^{-1}]	c	p	q	r_{min} [nm]	Φ_{min} [eV]
Ni-Ni	5.164	3.757	3.726	2.540	6.376	5.988	0.272	-0.140
Ni-B	2.586	3.854	3.726	2.500	4.818	4.422	0.218	-0.273
B-B	0.765	3.672	3.726	2.000	10.51	6.995	0.309	-0.026

FIG. 2. Neutron-weighted vibrational density of states $J(\omega)$. The solid curve gives the data determined from the velocity autocorrelation functions averaged over 201 MD simulations of 7 ps at 304 K. The squares give the experimental data from Lustig *et al.* (Ref. 21). Both curves are normalized to the same area.

of type n can be calculated by taking the Fourier transform of the corresponding velocity autocorrelation function obtained from a constant temperature simulation. From the two distributions $J_{Ni}(\omega)$ and $J_B(\omega)$ we can determine the neutron-weighted total vibrational density of states $J(\omega)$ according to

$$J(\omega) \propto \sum_n \frac{c_n b_n^2 J_n(\omega)}{m_n}, \quad (3)$$

where the sum is taken over all elements n, m_n is the atomic mass, b_n is the coherent scattering length for neutrons ($b_{Ni}=1.03\times10^{-14}$ m, $b_B=0.6\times10^{-14}$ m),[19] and c_n is the molar concentration.[20] In Fig. 2 the normalized density of states for the model system at $T=304$ K is shown together with the experimental data of Lustig *et al.*[21] The shoulder on the main peak is more pronounced for the simulation than for the experiment, causing the first observed maximum to be lower and the second to be higher. The reason for this is unknown. Nevertheless, both maxima are situated at the correct frequencies and the overall agreement is satisfactory.

The model system undergoes a glass transition at $T_g \approx 610$ K, which can be clearly seen in Fig. 3, where the number density ρ, the Wendt-Abraham ratios W_{NiNi} and W_{NiB}, and the time-averaged pair potential energy per atom $\langle u\rangle_{N,t}$ are plotted versus temperature. The Wendt-Abraham ratio $W_{nn'}=g_{nn'}(r_{\min 1})/g_{nn'}(r_{\max 1})$ is the ratio of first minimum, at $r=r_{\min 1}$, and the first maximum, at $r=r_{\max 1}$, of the pair correlation function $g_{nn'}(r)$, which is readily obtained from partial reduced radial distribution function $G_{nn'}(r)$. The Wendt-Abraham ratio is a measure for the degree of order in the nearest-neighbor shell. The glass transition temperature is within the experimentally observed range of transition temperatures for Ni-based glasses. Omitting the cohesive contribution to the total potential energy, the specific heat below the glass transition temperature is found to be 26.0 J mol^{-1} K^{-1}, only slightly larger than the classical value $3R$ (24.9 J mol^{-1} K^{-1}). This indicates that the combined temperature and density dependence of the cohesive contribution is small. The linear thermal expansion
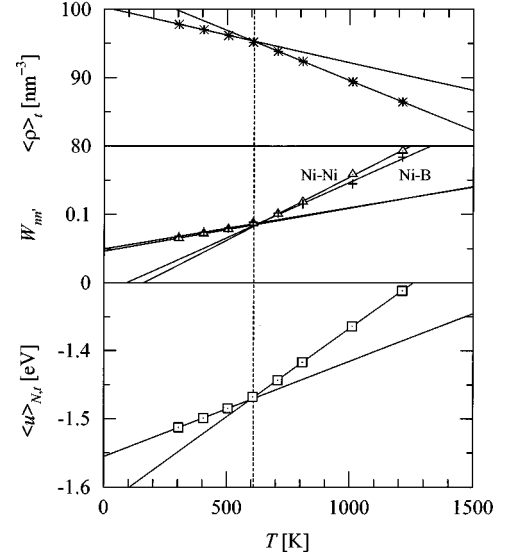

FIG. 3. The glass transition as evidenced by a change in slope of the time-averaged number density ρ (*), the Wendt-Abraham ratios W_{NiNi} ($\triangle$) and W_{NiB} (+), and the time-averaged pair potential energy per atom $\langle u\rangle_{N,t}$ ($\square$) as a function of temperature.

coefficient has a reasonable value of 2.78×10^{-5} K^{-1}. We conclude that our system has realistic glassy properties and shows a good agreement with the available experimental data.

IV. LAUNCHING A VIBRATIONAL MODE

In the harmonic approximation the vibrational modes of a system can be derived from the so-called dynamical matrix $\mathbf{D}$, which depends on the pair potentials and the atomic positions and masses.[22] Solving the eigenvalue problem $\omega^2\mathbf{B}=\mathbf{D}\cdot\mathbf{B}$ results in $3N$ eigenfrequencies ω_j and $3N$ eigenvectors $\mathbf{B}_j$ of length $3N$. After reweighting for mass, $\mathbf{B}_j$ is a concatenation of N relative amplitude eigenvectors $\mathbf{a}_j^i$, normalized according to

$$|\mathbf{B}_j| = \sum_{i=1}^{N} \sqrt{m^i}|\mathbf{a}_j^i| = 1 \quad \text{kg}^{1/2} \text{ m}, \quad (4)$$

in which m^i is the mass of atom i. Note that only the directions and the relative lengths of $\mathbf{a}_j^i$ are of importance. The matrix $\mathbf{D}$ is calculated for a system with the atoms at their equilibrium positions. These positions are obtained for a system at temperature T as follows: at $t=0$ s, the set point for the system thermostat is set at 50 K and all velocities are set to zero. In a simulation of 3.5 ps the thermostat is then programmed to cool the system to $T=0$ K with $dT/dt=-1.43\times10^{13}$ K s^{-1}. The resulting temperature initially rises above 50 K and then decreases towards 0 K. At $t=3.5$ ps the system has a temperature on the order of 10^{-1} K. In a subsequent simulation of 3.5 ps the temperature control (set to 0 K) proceeds to cool the system, resulting in a final temperature about 10^{-5} K.

A measure for the distribution of the magnitudes of the atomic vibrational amplitudes in a certain mode j is given by the participation ratio
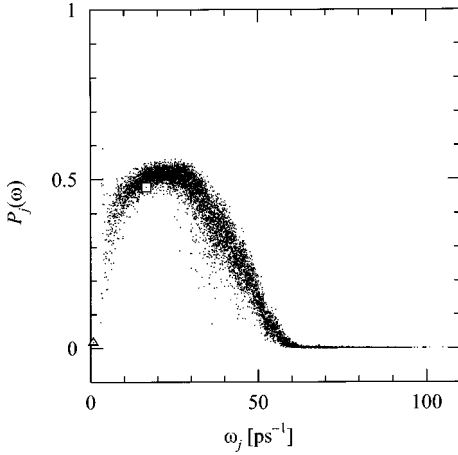
FIG. 4. Participation ratio versus eigenfrequency for a configuration at 506 K. Two modes that are discussed in this work are explicitly indicated: the randomly selected nonlocalized mode A by a square, the low-frequency localized mode B by a triangle.

$$P_j = \left(\sum_{i=1}^{N} |\mathbf{a}_j^i|^2 \right)^2 \bigg/ N \sum_{i=1}^{N} |\mathbf{a}_j^i|^4. \tag{5}$$

This ratio ranges from $1/N$ (all $|\mathbf{a}_j^i|=0$, except one) to unity (all $|\mathbf{a}_j^i|$ are equal). If for a certain vibrational mode P_j is small, only a few atoms have a considerable amplitude $\mathbf{a}_j^i$ for this mode, and the mode is called localized. As an example, the participation ratio versus eigenfrequency for a configuration at 506 K is shown in Fig. 4. The existence of low-frequency localized modes (for instance the triangle) is clearly visible.

After the determination of the vibrational spectrum a single vibrational mode j of the atomic configuration can be excited (''launched'') in a *constant energy* MD simulation. Located at their equilibrium positions at $t=0$, the atoms ($i = 1$ to N) are given an initial velocity

$$\mathbf{v}_j^i(0) = \alpha \mathbf{a}_j^i, \tag{6}$$

in which α is a launching constant. The proportionality between $\mathbf{v}_j^i(0)$ and $\mathbf{a}_j^i$ is consistent with the equation of motion in the harmonic approximation, so that this type of excitation is physically realistic. Note that no frequency is imposed on the system and that after being put into motion the atoms move on their own accord. The launching constant can have a positive or a negative value. We will use the sign of α to denote the initial ''direction'' of the vibration. The total energy that is supplied to the system to launch a mode is given by the initial kinetic energy
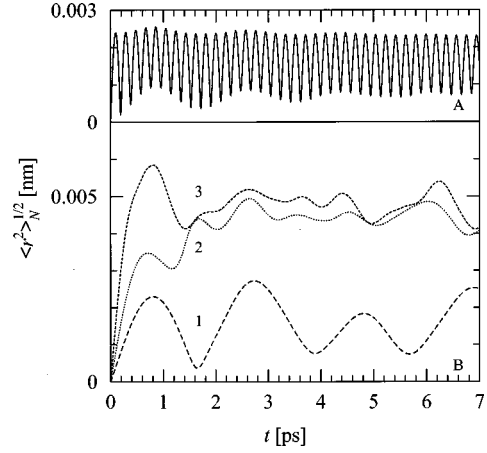

FIG. 5. Root mean square displacement of all atoms versus time for the launching of two vibrational modes: the nonlocalized mode A and the low-frequency localized mode B. The numbers along the curves denote launchings with different energies (see Table II).

$$K(0) = \sum_{i=1}^{N} k^i(0) = \sum_{i=1}^{N} \tfrac{1}{2} m^i |\mathbf{v}_j^i(0)|^2 = \tfrac{1}{2}\alpha^2 \sum_{i=1}^{N} m^i |\mathbf{a}_j^i|^2$$

$$= \tfrac{1}{2}\alpha^2 \ \text{m}^2 \ \text{kg}. \tag{7}$$

In this study the average initial kinetic energy per atom $\langle k(0) \rangle_N$ is in all cases less than 0.4 meV, which is very small compared to the average pair potential energy of the atoms at their equilibrium positions ($\langle u \rangle_N^{\text{eq}} \approx -1.55$ eV).

V. ATOMIC MOTION AFTER THE LAUNCHING OF A VIBRATIONAL MODE

We have determined the vibrational spectra of 21 atomic configurations obtained from an MD simulation at 506 K. From these spectra 151 low-frequency localized vibrational modes were studied ($\omega_j < 4.2$ ps^{-1} and $P_j < 0.15$). Four vibrational modes [one nonlocalized mode (denoted by A) and three low-frequency localized modes (B, C, D)] will be discussed in some detail. The launching data are collected in Table II. Figure 5 displays the root mean square (rms) displacement of all atoms after the launching versus time for the modes A and B. Mode A is an arbitrary *nonlocalized* mode (indicated by a square in Fig. 4) and is launched with an initial kinetic energy $K(0) = 1$ eV. The system vibrates almost perfectly harmonically. The frequency of the oscillations is $\omega = 16.514$ ps^{-1}, only slightly lower than the mode's harmonic eigenfrequency $\omega_j = 16.524$ ps^{-1}. The mode only slowly dissipates its energy to other modes.

In contrast, we find that launching a low-frequency *local-*

TABLE II. Eigenfrequencies, participation ratios, launching energies, and signs of the launching constants for the four selected vibrational modes.

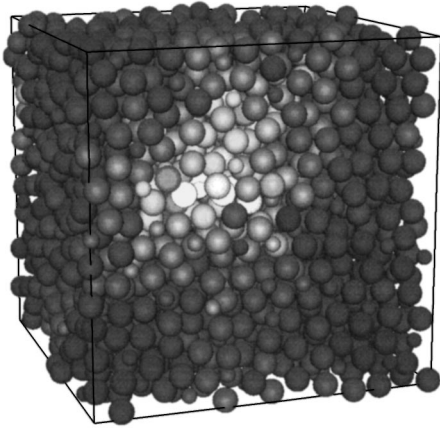| Mode	ω [ps^{-1}]	P	$K(0)$ [eV]					
			1	2	3	4	5	6
A	16.52	0.477	1+					
B	0.761	0.017	0.01+	0.04+	0.16+			
C	3.380	0.042	0.0025−	0.01−	0.04−	0.16+	0.8+	1.0+
D	2.154	0.013	0.04−	0.08−	0.16−	0.64−		

FIG. 6. The system after launch B2 (at $t=7$ ps). The greyscale indicates each atom's displacement from the initial position. All displacements are smaller than 0.12 nm.

FIG. 7. Projections d^i of the displacement vectors on the harmonic amplitude vectors versus time for the central atoms of launch B2.

ized mode does not result in a harmonic vibration but results in an anharmonic oscillation or in a jump. Mode B was taken from the same atomic configuration as the nonlocalized mode A, and is indicated by the triangle in Fig. 4. It is launched three times (B1, B2, B3) in the positive direction ($\alpha > 0$) with different initial kinetic energies (Table II). For the lowest launching energy (B1) the rms displacement only oscillates and therefore no persistent changes in the structure take place. The oscillation clearly deviates from harmonic behavior. Also, the frequency of the oscillations ($\omega \approx 0.25$ ps^{-1}) is much lower than the mode's harmonic eigenfrequency $\omega_j = 0.761$ ps^{-1}, which shows that the harmonic approximation is not valid for the launching of this mode at these amplitudes. For higher energies (B2, B3) jumps can be observed, after which the atoms vibrate around positions different from the initial ones. This points to the existence of a certain energy barrier for the jump, which in this case is somewhat less than 0.04 eV, the launching energy for B2 (Table II). Apparently, the breakdown of the harmonic approximation even at small amplitudes is a property of low-frequency localized modes. Instead of being harmonic the motion is anharmonic or can even result in a jump. The small difference in rms displacement between B2 and B3 is a result of the higher final temperature, causing an enhanced vibrational movement of all atoms. From Fig. 5 we can conclude that a configuration can move to a second potential-energy minimum when a low-frequency mode is launched out of its primary minimum. The fact that this second minimum is well defined is based on the following observations: (i) A threshold energy is required to induce a jump, (ii) After the jump the atoms vibrate around their newly obtained positions, (iii) The rms displacement after the jump is independent of the launching energy.

Until now we have only discussed the system as a whole. Closer inspection of the jump in real space reveals, not unexpectedly, that it is strongly localized (Fig. 6), at the same site as where the launched mode is localized. In order to make a certain distinction between atoms that are particularly susceptible to execute considerable motion and those that are not, from now on the 10 atoms that have the largest amplitude eigenvectors in a mode will be called the *central* atoms of this mode. The central atoms cause about 64 and
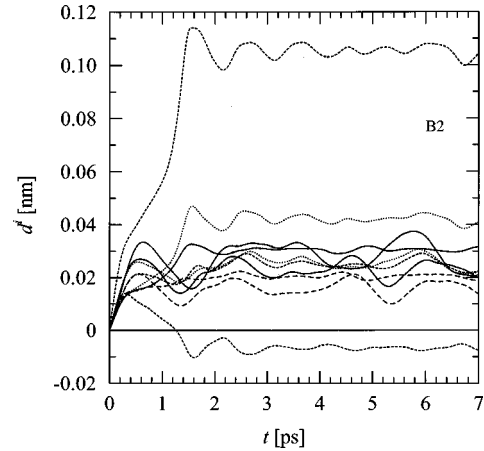
60 % of the total rms displacement for the launches B2 and B3, respectively. The projections $d^i(t) = \mathbf{r}^i(t) \cdot \mathbf{a}_j^i / |\mathbf{a}_j^i|$ of the atomic displacement vectors $\mathbf{r}^i(t)$ on the amplitude vectors $\mathbf{a}_j^i$ of these central atoms are shown in Fig. 7. Note the relatively small magnitudes of the jump distances (less than 0.12 nm) and their large spread: one atom even jumps in a direction opposite to its initial velocity. The jump has an unmistakably cooperative character: all atoms perform the jump in the same time interval of approximately 1.6 ps.

The movement resulting from the launching of mode B is typical for many localized low-frequency modes (see Sec. VII). For the two low-frequency localized modes C and D (Table II) that have a peculiar behavior, the rms displacements of the atoms after the launching are depicted in Fig. 8. These modes have been taken from configurations that are in all respects equivalent to the configuration of modes A and B. For the lowest launching energy (C1, D1) the motion is clearly anharmonic. Mode C is special because the launching of this mode in the positive (C5, C6) as well as in the negative direction (C2, C3) directly results in a jump. Mode C is therefore a triple-well location. The central atoms cause
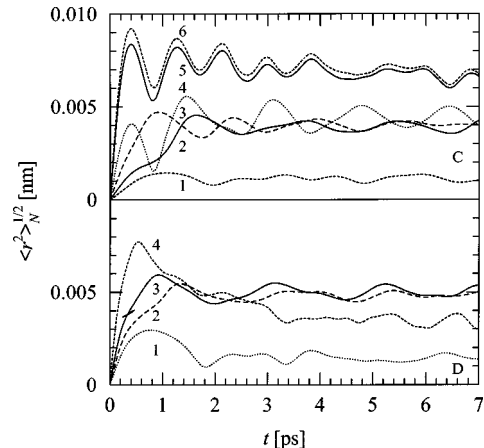

FIG. 8. Root mean square displacement of all atoms versus time for the launching of the two low-frequency localized vibrational modes C and D. The numbers along the curves denote launchings with different energies (see Table II).

about 61% of the total rms displacement for the launches in both directions. The launching of mode C in the positive direction with $K(0)=0.16$ eV (C4) does not result in a rms displacement equal to that of C5 and C6 (also launched in the positive direction). Instead, it results, after half an oscillation, in a jump with a rms displacement equal to that observed for the launches in the negative direction (C2 and C3). Apparently the launching energy for C4 is not enough to overcome the energy barrier in the positive direction, but as the oscillation proceeds, the remaining energy is large enough to overcome the energy barrier in the negative direction. More specifically, the energy barrier in the positive direction is thus found to be larger than 0.16 eV, whereas in the negative direction it is less than 0.01 eV.

Launching mode D results for the three lowest energies (D1, D2, D3) in a similar behavior as the launching of mode B. Again the central atoms cause about 60% of the total rms displacement. However, launching mode D with a higher energy (D4) results in a jump that is followed by a slow drift backwards. Closer inspection of this configuration at $t=7$ ps reveals that none of the atoms has moved over a considerable distance (all displacements are less than 0.02 nm) and that the central atoms cause only about 6% of the total rms displacement. Therefore no jump has occurred and the remaining difference in rms displacement between D1 and D4 is merely a result of the higher final temperature, similar to the rms differences between B2 and B3 and C5 and C6. Apparently, the energy barrier for the backward movement is smaller than the energy remaining after the jump, which allows the atoms to move back into the original potential-energy well.

VI. REVERSIBILITY

After completion of the forward jumps, the vibrational spectra of the configurations at $t=7$ ps were calculated. In the case of modes B and C these spectra no longer contain a low-frequency mode localized at the same location as the one that was launched. Therefore, the system could not be made to jump back to its original state by the procedure of localized-mode launching. Furthermore, attempts to induce backward jumps by launching the configurations after the jump with velocities opposite to the initial launching velocities also failed, using launching energies up to 1 eV. Obviously the initial jumps were irreversible, creating a structure lacking the possibility of a backward jump. However, other low-frequency localized modes did appear at different locations in the structure. The structure therefore still shows the same characteristics and has equivalent possibilities for atomic motion.

In contrast with the vibrational spectra of the configurations of modes B and C after the jump, the spectrum after launching mode D does contain a low-frequency localized mode at the same site, which does result in a backward jump when launched. Also the second type of attempt to induce a backward jump, using velocities opposite to the initial directions with $K(0)=0.04$ eV, succeeded. Reverse launching with $K(0)=0.01$ eV did not result in a backward jump. Note that for this mode the initial launching D4 $[K(0)=0.64$ eV] already resulted in a backward jump, whereas such a backward jump did not occur during the initial launching of modes B and C with energies up to 1 eV. Thus, launching mode D with sufficient energy results in a revers-

ible jump: it creates a structure containing a low-frequency localized mode which, when launched, recreates the original structure (apart from thermal displacements) including the original low-frequency localized mode D.

VII. RELAXATIONS, TWO-LEVEL STATES, AND DIFFUSION

Of the 151 low-frequency localized vibrational modes that have been studied, 2 modes show a reversible jump and 37 modes result in an irreversible jump when launched. The modes were launched with initial kinetic energies up to 1 eV, and the observed energy barriers range from 0.01 up to 1 eV. The 37 irreversible modes include 3 modes that are located at a triple-well location. Not all the low-frequency localized modes are located at a single location in the configuration; some appear to have more than one center. This was also observed by Schober and Laird in a MD soft spheres model.[7] Furthermore, the vibrational spectrum of a configuration can have multiple low-frequency localized modes with one to four common central atoms, which can lead to the occurrence of a common jump when one of the modes is launched. Therefore the launchings of the 37 irreversible modes led to only 25 distinguishable jumps. All observed atomic jump distances are smaller than 0.09 or 0.18 nm for Ni or B atoms, respectively, and all jumps have a cooperative character.

The TLS theory does not give an indication of the type of local geometry that gives rise to the presence of TLS's. The double potential-energy minima that are observed in our system conform to the description of a TLS, and therefore the likely conclusion is that in our system TLS's are located at the same sites as low-frequency localized modes that can cause a jump. Although we perform classical simulations, it is not unrealistic to envision atomic tunneling taking place at these sites. An important distinction is found in the effect of atomic motion on a TLS. In some cases the atomic motion at the TLS is reversible, a situation nicely fitting into the TLS picture. However, in the majority of cases the TLS has disappeared after the jump. These are the irreversible jumps, and this is an aspect of the behavior of TLS's that is not considered in the TLS theory. Experimentally, in addition to TLS's one also observes thermal local relaxations and (harmonic) vibrations, which become increasingly anharmonic towards lower frequencies. The general connection between thermal local relaxations and low-frequency localized modes was already shown by Oligschleger and Schober.[11] They report the occurrence of reversible and irreversible relaxations, but give no description of the mechanisms involved. We find that relaxations, i.e., cooperative jumps of the system from one potential-energy minimum to the next, can take place at sites where low-frequency localized modes are located. The relaxations can be of a reversible or an irreversible nature. In this picture the experimentally observed anharmonic vibrations are identical to low-frequency localized modes that will not cause a relaxation or that do not have enough kinetic energy to cause a relaxation.

In this work we have looked at individual vibrational modes. Yet, from the evidence obtained so far we can sketch a picture of the dynamics in the glassy state at elevated temperature. At each instant the system consists of a large collection of vibrational modes. The majority of these modes are nonlocalized and give rise to overall vibrational motion.
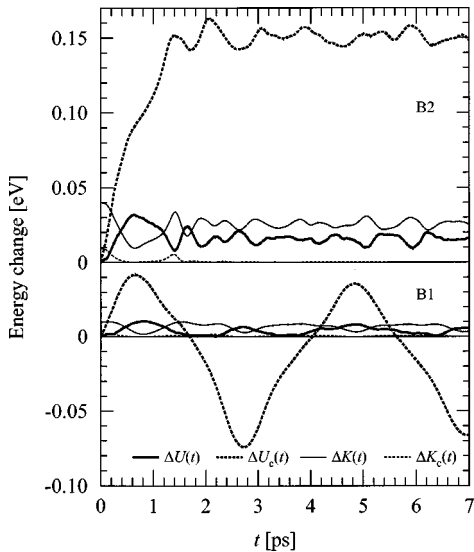
FIG. 9. Changes in the total pair potential energy $\Delta U(t)$ and the total kinetic energy $K(t)$ (solid curves), and the changes in the pair potential energy $\Delta U_c(t)$ and the kinetic energy $K_c(t)$ summed over the central atoms (dashed curves), for the launches B1 and B2.

A few low-frequency modes are localized, and each allows atomic motion at a particular spot in the system. At such a location the potential energy landscape shows considerable deviations from harmonicity; in the language of materials science one would speak of a defect. Naturally the atoms around the defect participate also in nonlocalized modes, but the resulting motion has much smaller amplitudes. It is the concentrated contribution from the low-frequency modes that can set a group of atoms into a particular kind of motion which has all the characteristics of a cooperative jump towards a new configuration. Seen in this way, diffusion in amorphous materials can very well be governed by the mechanism of groups of atoms executing such jumps. The jump distance is smaller than an atomic diameter, but several atoms move at the same time.

VIII. ATOMIC AND VIBRATIONAL MODE ENERGIES

Simulations following a launch are performed at constant energy and start from a configuration with all atoms at their equilibrium positions. The changes in the total (sum over *all* atoms) pair potential energy $\Delta U(t)$ and the total kinetic energy $K(t)$ as a result of the launching have to satisfy $\Delta U(t) + K(t) = K(0)$. Moreover, if no structural rearrangements take place and the oscillations deviate not too much from harmonic behavior, the time-averaged energy changes are governed by the equipartition principle $\langle \Delta U \rangle_t = \langle K \rangle_t$. Figure 9 shows that this is indeed the case for a launch not resulting in a jump (B1), as both solid lines vary around the same average value. The structural rearrangements that take place when a jump occurs (B2) result in a lower total pair potential energy than expected on the basis of the initial kinetic energy. Note that this decrease is only small. We have also observed modes whose launching results in a total pair potential-energy increase. For all irreversible jumps we find that directly after the launching the total pair potential energy goes through a maximum (at $t \approx 0.6$ ps) and the initial

kinetic energy $K(0)$ is thus used to cross an energy barrier (see Fig. 9).

The changes in the central (sum over the *central* atoms) pair potential energy $\Delta U_c(t)$ and the central kinetic energy $K_c(t)$ are also shown in Fig. 9 (dashed lines). The launch resulting in a jump shows a significant increase in the central pair potential energy, whereas the other launch does not. Note that the increase in the central pair potential energy $\Delta U_c(t)$ due to the jump is much larger than the initial central kinetic energy $K_c(0)$ and that the curve does not show a clear maximum. We have observed other irreversible jumps that do have a clear maximum in $\Delta U_c(t)$ and jumps that result in an immediate decrease of $\Delta U_c(t)$, thus showing a local downward slope in the energy. However, there is always an energy barrier present in the *total* pair potential energy $\Delta U(t)$.

If in a certain configuration all atoms are at their equilibrium positions, the total potential energy is in its minimum and any movement of a single atom will cause the total potential energy to be raised. We could picture this as each atom sitting at the bottom of its private potential well. When we introduce kinetic energy an atom will move up the slope of its well, thus increasing its potential energy. However, this picture is only true if the energy landscape remains unchanged, which is only the case if we keep all other atoms fixed. If the other atoms have movements of their own, the atom in question can have its potential energy lowered, even though it is moving up the slope of its well, because the well itself changes due to the motion of the neighboring atoms. Launching a low-frequency localized mode causes such changes in the local potential landscape. This can be seen in Fig. 9 for the launch B1, for which no jump occurs. The pair potential energy of the central atoms is not always larger than the equilibrium value $[\Delta U_c(t) > 0]$, but there are periods in which it is smaller. Furthermore, the fluctuations in $\Delta U_c(t)$ can be much larger than the fluctuations in $\Delta U(t)$. Thus changes in the potential energy of the central atoms must be supplied by or taken up by the $N-10$ noncentral atoms. This explains why a small group of atoms can execute a jump to a higher pair potential energy even though the amount of energy given to those atoms at the launch is considerably smaller than the pair potential energy increase. The energy graphs in Fig. 9 indicate not only that the ten central atoms jump simultaneously but also that this jump is possible only thanks to cooperation of the other atoms in the system. From Fig. 9 it can be concluded that if launch B1 were performed in the opposite direction the central atoms would have their pair potential energy decreased immediately. The reason why the structure nevertheless considers the starting points of these ten atoms as their equilibrium positions is because in order to move in the direction of the lower potential energy the surrounding atoms have to move in directions of higher potential energy and this increase is greater than the possible energy decrease of the central atoms.

The pair potential and kinetic energies for the launching of mode D, which can exhibit a reversible jump when launched, are shown in Fig. 10. If no jump occurs (D1), again all long-time energy changes are governed by the equipartition principle, and again the fluctuations in the pair potential energy of the central atoms are much larger than the pair potential-energy difference for all atoms and larger than the central launching energy. After the jump (D2) the total
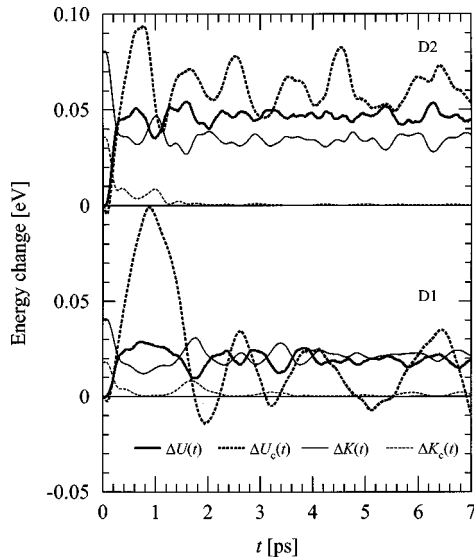
FIG. 10. Changes in the total pair potential energy $\Delta U(t)$ and the total kinetic energy $K(t)$ (solid curves), and the changes in the pair potential energy $\Delta U_c(t)$ and the kinetic energy $K_c(t)$ summed over the central atoms (dashed curves), for the launches D1 and D2.

pair potential energy has increased with respect to $\langle K \rangle_t$. Immediately after the launching the pair potential energy does not show a distinct maximum and although an energy barrier for the backward jump must be present (the configuration after the jump is stable), we do not observe it in Fig. 10. An energy maximum in $\Delta U_c(t)$ is visible at $t \approx 0.7$ ps, but just as for a reversible jump, the initial central launching energy is smaller than the energy maximum and therefore the noncentral atoms again have a crucial influence. The other observed low-frequency mode that can cause a reversible jump (not shown) also shows a central potential-energy maximum and has no visible energy barrier. The structural difference

between a site where a reversible jump can take place and one where an irreversible jump can take place is apparently related to the size of the energy barrier and possibly also connected to the presence of a central potential energy maximum. The reason for this behavior is not known.

IX. CONCLUSIONS

A computational model of a metallic glass clearly shows the existence of two-level states. These double potential-energy wells are located at the same sites as low-frequency localized vibrational modes. The launching (excitation) of such a mode causes the potential-energy landscape to change and can lead to a jump into the nearby potential-energy minimum. The jumps have a cooperative character involving some tens of atoms, some of which gain potential energy in the process whereas others lose energy. The potential-energy exchange among the atoms located at the jump site can be considerably larger than the total introduced excitation energy. The jump can be of a reversible or an irreversible nature, and a distinction can be made between two-level states that allow reversible atomic motion to take place and two-level states that disappear after the jump. The jumps can be identified with the local relaxations that have been predicted to occur in amorphous materials between 2 to 10 K. The vibrations of low-frequency localized modes that do not cause a relaxation correspond to the experimentally observed anharmonic vibrations.

[1] R. C. Zeller and R. O. Pohl, Phys. Rev. B **4**, 2019 (1971).

[2] *Amorphous Solids: Low Temperature Properties*, edited by W. A. Phillips (Springer, Berlin, 1981).

[3] W. A. Phillips, Rep. Prog. Phys. **50**, 1657 (1987).

[4] U. Buchenau, H. M. Zhou, N. Nücker, K. S. Gilroy, and W. A. Phillips, Phys. Rev. Lett. **60**, 1318 (1988).

[5] J.-B. Suck and H. Rudin, in *Glassy Materials II*, edited by H. Beck and H.-J. Güntherodt (Springer, Berlin, 1983), p. 217.

[6] U. Buchenau, Y. M. Galperin, V. L. Gurevich, and H. R. Schober, Phys. Rev. B **43**, 5039 (1991).

[7] H. R. Schober and B. B. Laird, Phys. Rev. B **44**, 6746 (1991).

[8] J. Hafner, M. Krajcí, and M. Windisch, J. Non-Cryst. Solids **192−193**, 212 (1995).

[9] L. D. van Ee, B. J. Thijsse, and J. Sietsma, J. Non-Cryst. Solids **205−207**, 614 (1996).

[10] L. Guttman and S. M. Rahman, Phys. Rev. B **33**, 1506 (1986).

[11] C. Oligschleger and H. R. Schober, Solid State Commun. **93**, 1031 (1995).

[12] T. A. Weber and F. H. Stillinger, Phys. Rev. B **31**, 1954 (1985).

[13] Ch. Hausleitner and J. Hafner, Phys. Rev. B **47**, 5689 (1993).

[14] J. C. Li, N. Cowlam, and F. He, J. Non-Cryst. Solids **112**, 101 (1989).

[15] B. J. Thijsse, L. D. van Ee, and J. Sietsma, in *Crystallization and Related Phenomena in Amorphous Materials,* edited by M. Libera, T. E. Haynes, P. Cebe, and J. E. Dickinson, Jr., MRS Symposia Proceedings No. 321 (Materials Research Society, Pittsburgh, 1994), p. 65.

[16] P. Lamparter, W. Sperl, S. Steeb, and J. Blétry, Z. Naturforsch. A **37**, 1223 (1982).

[17] R. L. McGreevy and L. Pusztai, Mol. Simul. **1**, 359 (1988).

[18] E. W. Iparraguirre, J. Sietsma, B. J. Thijsse, and L. Pusztai, Comput. Mater. Sci. **1**, 110 (1993).

[19] G. E. Bacon, *Neutron Diffraction*, 3rd ed. (Clarendon, Oxford, 1975).

[20] N. Lustig, J. S. Lannin, J. M. Carpenter, and R. Hasegawa, Phys. Rev. B **32**, 2778 (1985).

[21] N. Lustig, J. S. Lannin, and R. Hasegawa, Phys. Rev. B **34**, 6725 (1986).

[22] P. H. Dederichs and R. Zeller, in *Point Defects in Metals II, Vol. 87 of Springer Tracts in Modern Physics,* edited by G. Höhler (Springer-Verlag, Berlin, 1980).